Flood mapping: a methodology based on mathematical modelling and satellite imaging

R.B. CANELAS*, A.J.C. CRESPO, M.L. FERREIRA, M. GÓMEZ-GESTEIRA
**ricardo.canelas@ist.utl.pt*
CEHIDRO, Instituto Superior Técnico
ULisbon, Lisbon, Portugal

ABSTRACT

A 2DH mathematical model assembled at CEHIDRO, IST, is employed to model 2000/2001 Tagus river floods over a 70 km reach, with the key objective to assess its performance envisaging its use as a forecasting tool. The model is suited for highly unsteady discontinuous flows over complex geometries, employing a finite-volume discretization scheme, based on a flux-splitting technique incorporating a reviewed version of the Roe Riemann solver. New boundary conditions were developed, based in the Riemann invariant, in order to cope with the provided hydrographs in a mathematically coherent manner. Detailed discharges and water levels are available for the inlet and outlet sections, as well as for the inlet at river Zêzere, a Tagus affluent. A high resolution Digital Elevation Model (DEM) is used. Spatially heterogeneous roughness characteristics are derived from land-use databases built from satellite data.
Synthetic Aperture Radar (SAR) satellite imagery of the floods is available and is used to validate the simulation results. The delimited areas from the satellite and simulations are over imposed and show a very good agreement in all major flood extents, with small structures, with lengths at the order of the spatial discretization, clearly reproduced. Flow depths and registered discharges are recovered from the simulation and compared with data from a measuring station in the domain. The comparison shows remarkably high accuracy, both in terms of amplitudes and phase. Further calibration of the roughness parameters and inclusion of detailed terrain structures like small levees should improve the flood extents regarding the comparisons with satellite data.

keywords: Flood modeling, SAR, Finite-volume, Calibration.

1. Introduction

Flood events may have an important impact on human societies due to their considerable destructive potential. The existence of communities in flood plains, due to advantageous natural conditions, increases the risk dramatically. Flood mitigation is, therefore, an extremely important investment but also a complex task that no single measure can tackle. As such, extensive knowledge of the flood temporal and spatial extensions are of superior importance to derive an array of solutions aiming to mitigate the risk of such events.
Flood modeling can contribute to a response to such requests, in the sense that reach scale flood events can be modeled and the desired information collected at a very low cost. Such endeavor requires, from the numerical model, the ability to consider unsteady flows over complex topography. Two-dimensional depth-averaged (2DH) models have

been extensively described in the engineering literature but there are, however, some open topics on how to deal with difficulties that natural channel geometries pose. Nonetheless, several models are used and continue to be developed and calibrated (Bates *et al*, 1998; Horritt, 2000; Hall *et al*, 2011). 2DH models are usually regarded as tools to more detailed studies of short reaches and small duration events. However, relevant speed-ups resorting to code parallelization, taking advantage of multi-core processors or dedicated accelerators, mesoscale simulations resolved to the reach scale, spanning several days or weeks periods are now feasible.

This works is an application of the Strong Transients in Alluvial Valleys 2D (STAV2D) code, a model that relies on a Finite-Volume Method (FVM) discretization (LeVeque, 2002). It employs a technique first presented by Murillo & García-Navarro (2010), where the discretization of the non-homogenous terms of hyperbolic systems of conservation laws is made in ways compatible with steady solutions, such as still water in hydrostatic equilibrium or steady flows in complex, natural bed geometries. Bed slope source terms are of special importance in this case and for that reason considerable effort has been devoted to the topic of correctly including them in the scheme, preserving the properties of the homogeneous equations.

The Tagus case-study represents a challenge due to the geometry and dimension of the reach under consideration, as well as the combination of flood plains and steep terrain in the DEM and the duration of the events.

The objective of this work is to model historic events on the considered domain using the STAV2D model, in an attempt to assess the possibility of its employment as a forecasting tool. Two concerns arise considering the base data that the model uses: the quality of the geometry and the roughness parameters. The DEM must be sufficiently similar to the current geometry, a difficult requirement considering the intensity of geomorphic activity in river systems. The roughness estimates, derived from crossing data from the literature (Mattocks, 2006; Chow, 1959; Kalyanapu, 2009) and the CORINE Land Cover Project data, are given for uniform flows and very different values can be assigned to similar areas while maintaining consistency with the literature.

The novelty of the work arises from the boundary conditions, derived as to allow for complex, regime changing scenarios, the size and resolution of the simulation and the usage of satellite imagery to provide cues regarding the simulation results.

2. Conservation Equations and Closure Models

The application of the Reynolds Transport Theorem (RTT) to the quantities total mass and momentum in both directions yields

$$\partial_t h + \partial_x \left(hu\right) + \partial_y \left(hv\right) = 0 \tag{1}$$

$$\partial_t \left(uh\right) + \partial_x \left(u^2 h + \frac{1}{2} g h^2 \right) + \tag{2}$$

$$+ \partial_y \left(uvh\right) = -gh\partial_x Z_b - \frac{\tau_{b,x}}{\rho}$$

$$\partial_t \left(vh\right) + \partial_x \left(uvh\right) + \partial_y \left(v^2 h + \frac{1}{2} g h^2 \right) = \tag{3}$$

$$= -gh\partial_y Z_b - \frac{\tau_{b,y}}{\rho}$$

where h is the fluid height above the bed elevation, g is the acceleration due to gravity, u and v are the depth-averaged velocities in the x and y directions, respectively and Z_b is the bed elevation. In equations (2) and (3), ρ is the

density, $\partial_{x_i}(Z_b)$ represents the bottom slope contribution for the momentum, and $\boldsymbol{\tau}_{b,i}$ is the bed shear stress.
The bed shear stress, $\boldsymbol{\tau}_b$ is such that

$$|\boldsymbol{\tau}_{\mathbf{b}}| = \rho C_f |\mathbf{u}|^2 \quad (4)$$

and the friction coefficient, C_f, in order to reproduce the Manning-Stricler formula, is expressed as $C_f = g/K_s^2 h^{1/3}$, where K_s is the Strickler parameter, the inverse of the Manning coefficient.

3. Discretization Scheme

The set of conservation laws (1) to (3) configures a 1st order hyperbolic, non-homogeneous, quasi-linear system of partial differential equations that can be written in compact vectorial notation as

$$\partial_t\left(\mathbf{U}(\mathbf{V})\right) + \nabla\cdot\mathbf{E}\left(\mathbf{V}\right) = \mathbf{R}\left(\mathbf{V}\right) + \mathbf{T}\left(\mathbf{V}\right), \quad (5)$$

where $\mathbf{V} = \left[h\ u\ v\right]^{\mathrm{T}}$ and $\mathbf{U} = \left[h\ \ uh\ \ vh\ \right]^{\mathrm{T}}$ are the vectors of primitive and conservative variables, respectively, $\nabla\cdot\mathbf{E}$ is given by $\nabla\cdot\mathbf{E} = \partial_x\mathbf{F} + \partial_y\mathbf{G}$, $\mathbf{F} = \left[uh\ \ u^2h + 1/2gh^2\ \ uvh\right]^{\mathrm{T}}$, $\mathbf{G} = \left[vh\ \ vuh\ \ v^2h + 1/2gh^2\right]^{\mathrm{T}}$ are the flux vectors, $\mathbf{R} = \left[0\ \ -gh\partial_x Z_b\ \ -gh\partial_y Z_b\right]^{\mathrm{T}}$ is the vector of non-conservative fluxes and $\mathbf{T} = \left[-\partial_t Z_b\ \ -\tau_x/\rho\ \ -\tau_y/\rho\right]^{\mathrm{T}}$ is a source vector.
To obtain the Finite Volume (FV) discretization, system (5) is integrated in a cell I. The Gauss theorem is applied to the divergence terms resulting in

$$A_I \frac{\Delta\left\langle \mathbf{U}_I \right\rangle}{\Delta t} + \sum_{K=1}^{N_I} L_{IK}\Delta_{IK}\left(\left(\mathbf{E}-\mathbf{R}\right)\cdot\mathbf{n}_{IK}\right) = A_I\left\langle \mathbf{T}_I \right\rangle, \quad (6)$$

where A_I is the area of cell I, L_{I_K} is the length of edge K of cell I, N_I is the number of edges of cell($N_I = 3$ in this case) I, Δ_{IK} represents the variation across the K^{th} edge of cell I and $\mathbf{n}_{IK} = (n_x, n_y)^T$ is the outward unit normal vector to each K edge of the cell I. Operator $\langle\ \rangle$ represents the spatial average over the cell area. The flux variation across the K^{th} edge of cell I, $\Delta_{IK}\left(\left(\mathbf{E}-\mathbf{R}\right)\cdot\mathbf{n}_{IK}\right)$, is expressed as a function of the local variation of the dependent conservative variables, using Roe's approximate Riemann solvers (Roe, 1981). Note that the flux vector of a system of shallow-flow conservation laws is not homogeneous and, hence, it is not possible to perform an exact flux vector splitting. Assuming a local linearization of the flux vectors orthogonal to an edge, one obtains

$$\begin{aligned}\Delta_{IK}\left(\mathbf{E}\cdot\mathbf{n}_{IK}\right) &= \sum_{m=1}^{3} \tilde{\lambda}_{IK}^{(m)}\,\alpha_{IK}^{(m)}\,\tilde{\mathbf{e}}_{IK}^{(m)} \\ \Delta_{IK}\left(\mathbf{R}\cdot\mathbf{n}_{IK}\right) &= \sum_{m=1}^{3} \beta_{IK}^{(m)}\,\tilde{\mathbf{e}}_{IK}^{(m)}\end{aligned} \quad (7)$$

(Toro, 2001; Murillo & García-Navarro, 2010), where $\alpha_{IK}^{(m)}$ are the wave-strengths for each of the eigenvectors $\tilde{\mathbf{e}}_{IK}^{(m)}$ and $\tilde{\lambda}_{IK}^{(m)}$ are the respective eigenvalues. The expressions of the wave-strengths, eigenvectors and eigenvalues are well known and can be consulted in Toro (2001), among others. $\beta_{IK}^{(m)}$ follows an expression that guarantees a well-balanced scheme and correct energy dissipation at jumps, derived by Murillo & García-Navarro (2010). The remaining source term, $\mathbf{T}$, is discretized in a point-wise, semi-implicit manner as $\mathbf{T}_I(t+\Delta t) \equiv \mathbf{T}_I^{n+1}$. It is computed in an intermediate step with the updated variables of the homogeneous part of equation (6). Bed shear stress is simply taken as(4). Introducing equations (7) into (6), this Godunov-type flux-splitting FV scheme can be summarized as

$$\mathbf{U}_I^{n+1} = \mathbf{U}_I^n - \\ -\frac{\Delta t}{A_I}\sum_{K=1}^{3} L_{IK}\sum_{m=1}^{3}\left(\tilde{\lambda}^{(m)}\alpha^{(m)} - \beta^{(m)}\right)^{-}_{IK}\tilde{\mathbf{e}}^{(m)}_{IK} + \\ +\Delta t\left(\mathbf{T}_I^{n+1}\right), \quad (8)$$

where only the negative part of the eigenvalues $\tilde{\lambda}^{(m)}_{IK}$ and of the wave-strengths $\alpha^{(m)}_{IK}$ and $\beta^{(m)}_{IK}$ are used, ensuring that only in-coming fluxes are considered in the update of the conserved variables.

When cell-averaging the solution, the time step is chosen small enough to guarantee that there is no interaction between waves obtained as the solution of the Riemann Problem (RP) at adjacent cells. The stability region considering the homogeneous part of the system resembles a traditional *CFL* condition, with added terms arising from the non-homogenous part (Murillo & García-Navarro, 2010). Wetting and drying algorithms, as well as the necessary entropy corrections in order to ensure that physical solutions are always attained in critical flow points are also drawn from (Murillo & García-Navarro, 2010).

3.1. Inlet/Outlet Boundary Conditions for River Modeling

1D information (discharge or level) must be transformed into 2D information (fluid height and velocity field) at the open boundaries. The characteristics method, employing the Riemann Invariant, is used on each edge associated to the characteristic line that leaves the domain at that edge identified as a permissive boundary. For the inlet case, assuming a frictionless bed, the Riemman Invariant can be written as

$$u_I - 2\sqrt{gh_I} = u_{I,g} - 2\sqrt{gh_{I,g}} \quad (9)$$

where $q_{KI,g}$ is the discharge associated with the boundary *K* edge of element I,g and L_{LI} is the respective length. Assuming that $u \propto h^{2/3}$ allows for the writing of

$$q_{KI,g} = L_{KI}h_{I,g}u_{I,g} = L_{KI}\alpha h_{I,g}^{5/3} \\ Q_{in} = \sum_I L_{KI}\alpha h_{I,g}^{5/3} \quad (10)$$

where Q_{in} is the total discharge. The solution algorithm consists of splitting Q_{in} into a series of $q_{KI,g}$ according to the cell fluid height, solving (9) in every inlet edge, finding a *h* distribution, and iteratively solve the new inlet level, taken as the average of the fluid levels of every wet cell. Once the new wet section is defined, (10) is solved in order to α and the velocity field (only existing in the normal to the inlet section) is imposed in the ghost cells. These cells are then used in equation (8) to update the rest of the domain.

The outlet solution strategy is similar, employing in this case the Riemann Invariant associated to the first characteristic field, written for a subcritical flow as

$$u_I + 2\sqrt{gh_I} = u_{I,g} + 2\sqrt{gh_{I,g}} \quad (11)$$

The solution in this case is simpler, since the flow level is imposed by the outlet condition and one needs only to use (11) to solve for a velocity distribution at the boundary. This condition is not required for supercritical flows crossing the outlet: there are no upstream travelling characteristic waves, all the information leaves the domain.

Both permissive conditions assume that there is no friction on the bed, as to simplify the computation of the Riemann Invariants. A frictionless buffer zone is set around these regions, also useful since the inlet condition

assumes a horizontal free surface in the cross section.

4. Results

4.1. Simulation setup

The domain consists of a 70 Km reach of the Tagus, Portugal, and approximately 10 Km of the Zêzere river, affluent of the Tagus. The considered area experiences regular floods and is monitored by 4 stations. The Tagus inlet is located at the Tramagal monitoring station cross section, with the outlet at the Ómnias station section. The Zêzere inlet is located at the Castelo-de-Bode station, and the fourth station, Almourol, is located 3 km downstream of the Tagus-Zêzere confluence. The discretization consists of an anisotropic unstructured mesh, *15 m* average side in the main channel and floodplains and a smooth gradient with respect to elevation from such areas, with the largest cell sizes of approximately *300 m*. This resulted in over 1.3×10^{6} mesh elements.

The Digital Elevation Map, in Figure 1, was obtained in 2008 and complemented with the major levee structures, mostly concentrating in the left banks. It was subsequently sampled to a resolution of 30 m and applied to the computational mesh. The roughness map was built based on the soil classification by the CORINE Land Cover project, using average Strickler coefficient values proposed in the literature (Mattocks, 2006), resulting in Figure 2. The initial conditions represent the steady state for the annual median flow, 450 m^3s^{-1} for the Tagus and 150 m^3s^{-1} for the Zêzere, imposed at the respective inlet sections, together with the respective level imposed at the outlet. Figures 3 and 4 represent the initial state, achieved by allowing the simulation to run for an extended period of time, until the total mass in the domain reached a constant value, as well as the time step, indicating that every flux is effectively balanced and permanent.

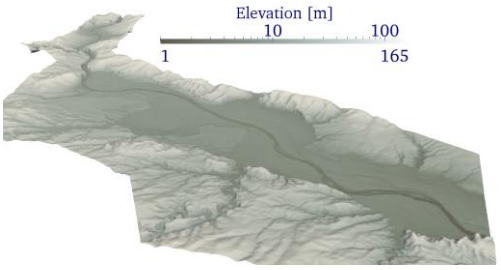

Fig. 1. View of the domain from downstream.

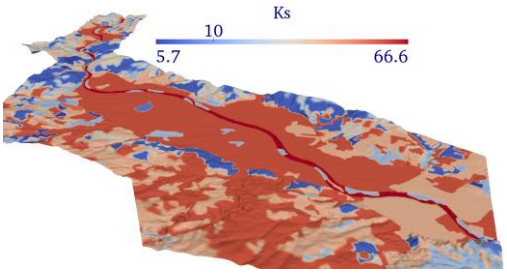

Fig. 2. Spatial distribution of the coefficient of Mannning Strickler's equation.

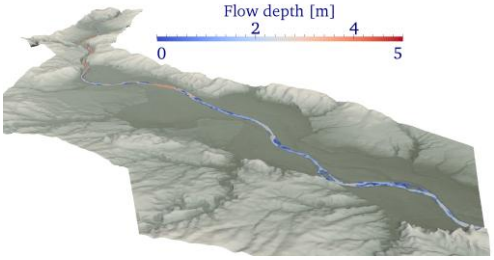

Fig. 3. Initial flow depth.

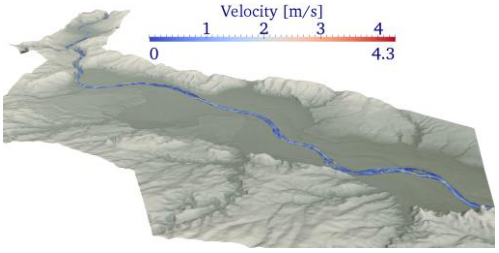

Fig. 4. Initial velocity field.

Two flood events were modeled, with simulation times from December 29th to January 9th 2001 and from the 5th to the 13th of February. The inflow hydrographs are represented in Figure 5. Satellite imagery is available for the 5th of January, 9th and 11th of February, marked by the vertical lines in Figure 5, covering the whole flood extents in the considered reach.

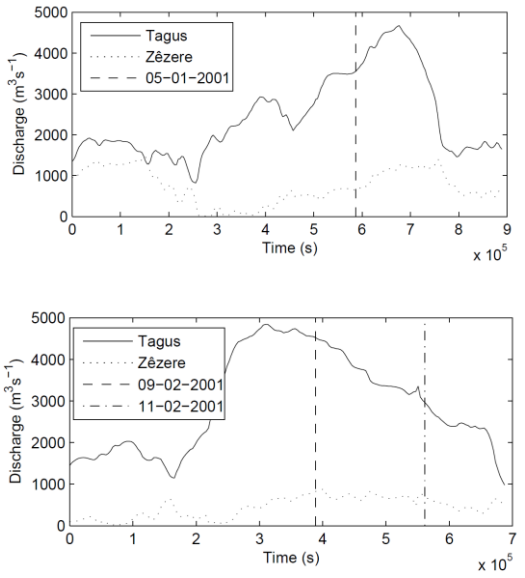

Fig. 5. Discharges at Tagus and Zêzere inlets; Top - December 29th to January 9th; Bottom - 5th to the 13th of February.

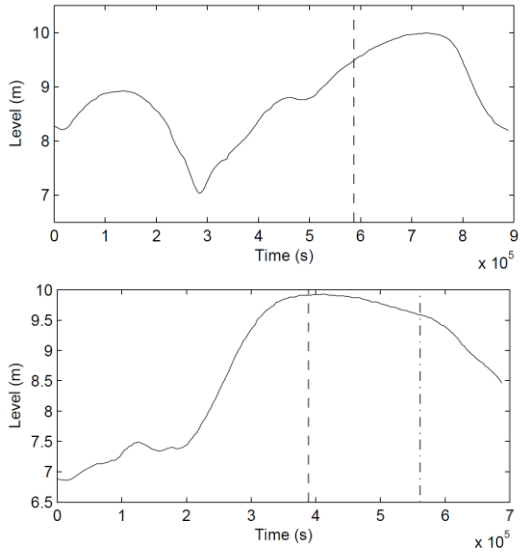

Fig. 6. Level at the Tagus outlet; Top - December 29th to January 9th; Bottom - 5th to the 13th of February.

4.2. Results

The results of the STAV2D model were compared with monitoring data and available satellite imagery. These results can however be considered blind tests, since no calibration effort was carried out.

Approximately 3 *km* downstream of the Tagus-Zêzere confluence is the Almourol monitoring station. The available data covers the considered event and several considerations can be drawn. Concerning mass conservation and wave celerities, the discharge in the Almourol section was computed and is compared in Figure 7 with the measurements at the station for both episodes.

The computed discharges correctly follow the measured curves, describing in detail every oscillation imposed by the inlet boundary conditions and the geometry for both cases. For $t < 5\times10^4 s$ the plot shows the fast rise of the discharge in order to cope with the difference between the permanent initial flow and the imposed conditions.

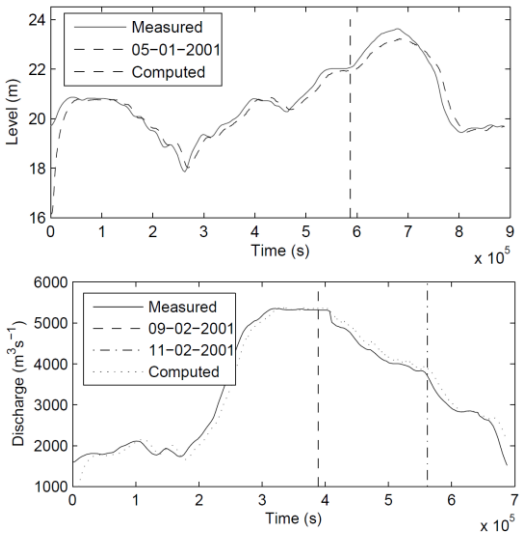

Fig. 7. Measured and computed discharges at Almourol monitoring station. Left - December 29th to January 9th; Right - 5th to the 13th of February

Friction parameters have a large influence on flow depth, and even if no

calibration is presented in this work, it is important to estimate the quality of the assumptions made concerning soil usage and its relation to rugosity coefficients. Figure 8 shows the measured and computed levels at Almourol station.

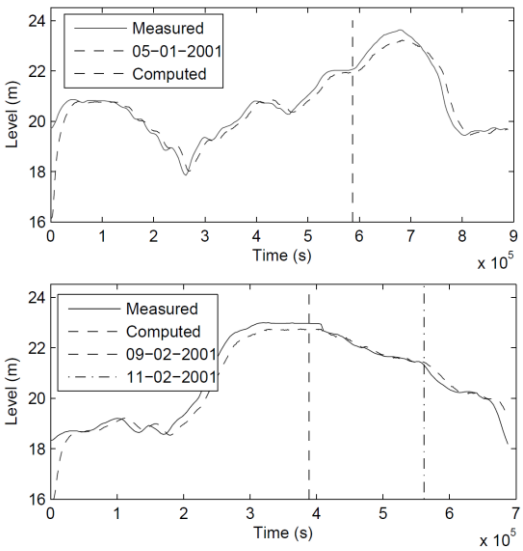

Fig. 8. Measured and computed water level at Almourol monitoring station. Left - December 29th to January 9th; Right - 5th to the 13th of February

The agreement of registered and computed values is similar to that regarding the discharge, indicating that the friction coefficient estimate was generally adequate. The peak levels present a superior deviation from the measured values. Regarding such deviation, the satellite imagery in Figures 9 and 10 presents some insights.

Fig. 9. White contour - Satellite image; Blue surface - Computed wet domain; Red line - Almourol section. 5th January.

Fig. 10. White contour - Satellite image; Blue surface - Computed wet domain; Red line - Almourol section. Top-8th February; Bottom - 5th January.

The simulated flood extent, although preserving the major structures of the observed flood, shows some discrepancies mainly at the left floodplain. The flood plains are used for agricultural purposes and the morphological impact of flood events is substantial in these areas. Small hydraulic works are also common, live levees and routing canals, carried out by the agricultural community. It is therefore hypothesized that most of the differences observed are a product of the differences in the actual terrain from 2001 and the year of the DEM survey. The algorithm used to extract the flood extent from satellite data may also produce artifacts that may explain smaller differences in other regions. The fact that the flooded area is virtually identical for most of the right bank

supports these hypotheses. At peak level, the discrepancies should also produce the stronger deviations between simulation and satellite data.

5. Conclusions

Fluvial modeling introduces several problems for a simple discretization of the shallow-flow equations. Fast evolving fixed (inflow and outflow) and free (wetting and drying) boundaries, as well as complex channel bed configurations demand special attention if a stable and accurate solution is to be computed. A state-of-the-art general shallow water model, STAV2D, based on the Finite Volume Method, is used. It employs an extended and reviewed version of Roe's solver. Different approaches to the integral source terms for the bed slope were used, ensuring that the model is well-balanced for hydrostatic and non-hydrostatic solutions, even in the presence of irregular bed geometry. The model is compatible with spatially heterogeneous roughness parameters. Mesh refinement is also naturally incorporated by the method.

STAV2D was used to model a flood in the Tagus river, Portugal. The efficiency of the discretization, as well as the implementation, allow for the modeling of a 70 km long reach, with an approximately 15 m resolution anisotropic unstructured grid, with an average ratio of 1.35 computing time to simulated time in an 8-core machine. This allows for detailed simulations of highly unsteady flows for extended periods of time in a normal desktop machine, with accessible programming tools.

Satellite imagery was used to assess the results from the model. The results appear to be consistent and indicate that the presented conceptual models and discretization are suitable for the modeling of this type of flood simulations. The possible calibration relies only on the roughness coefficients, both value and spatial distribution wise. Apart from the uncertainties in the DEM and the roughness parameters, the model provided accurate results and encourages future developments as a research and engineering tool.

References

Bates, P., Stewart, M., Siggers, G., Smith, C., Hervouet, J.-M. & Sellin, R. (1998). 'Internal and external validation of a two-dimensional finite element code for riverflood simulations', Proceedings of the Institute of Civil Engineers, Water, Maritime and Energy, 130.

Burguete, J. & García-Navarro, P. (2001). 'Efficient construction of high-resolution tvd conservative schemes for equations with source terms: application to shallow water flows', Int. Journal for Numerical Methods in Fluids, 37(2), 209-248.

Chow (1959). Open-Channel Hydraulics. McGraw-Hill. New York. ISBN 1-9328461-8-2

Hall, J. W., Manning, L. J. & Hankin, R. K. S. (2011). 'Bayesian calibration of a flood inundation model using spatial data', Water Resour. Res, 47.

Horritt, M. S. (2000). 'Calibration of a two-dimensional finite element flood flow model using satellite radar imagery', Water Resour. Res, 36.

Kalyanapu, A., Burian, S. & McPherson, T. (2009). 'Effect of land use-based surface roughness on hydrologic model output', Journal of Spatial Hydrology, 9.

Kurganov, A. & Petrova, G. (2007). 'A second-order well-balanced positivity preserving central-upwind scheme for the Saint-Venant system', Communications in Mathematical Sciences, 5, 133-160.

LeVeque, R. (2002). 'Finite Volume Methods for Hyperbolic Problems', Cambridge University Press.

Mattocks, C., Forbes, C. & Ran, L. (2006). 'Design and implementation of a real-time storm surge and flood forecasting capability for the state of North Carolina', UNC-CEP Technical Report.

Murillo, J. & García-Navarro, P. (2010). 'Weak solutions for partial differential equations with source terms: application to the shallow water equations', J. Comp. Physics, 229(11), 4327-4368.

Murillo, J., García-Navarro, P., Brufau, P. & Burguete, J. (2010). '2D modeling of erosion/deposition processes with suspended load using upwind finite volumes', Journal of Hydraulic Research, 46(1), 99-112.

Roe, P. (1981). 'Approximate Riemann solvers, parameter vectors and difference schemes', J. Comp. Physics, 43, 357-372.

Toro, E. (2001). 'Shock-Capturing Methods for Free Surface Shallow Flows', Wiley, New York.

Vázquez-Cendón, M. (1999). 'Improved treatment of source terms in upwind schemes for the shallow water equations with irregular geometry', J. Comp. Physics, 148(2), 497-526.